An Electronic Prosthesis Mimicking the Dynamic Vestibular Function

Andrei M. Shkel[a]

[a]University of California - Irvine, Department of Mechanical and Aerospace Engineering, 4208 Engineering Gateway, Irvine, CA, USA 92697

ABSTRACT

This paper reports our progress toward development of a unilateral vestibular prosthesis. The sensing element of the prosthesis is a custom designed one-axis MEMS gyroscope. Similarly to the natural semicircular canal, the microscopic gyroscope senses angular motion of the head and generates voltages proportional to the corresponding angular accelerations. Then, voltages are sent to the pulse generating unit where angular motion is translated into voltage pulses. The voltage pulses are converted into current pulses and are delivered through specially designed electrodes, conditioned to stimulate the corresponding vestibular nerve branch. Our preliminary experimental evaluations of the prosthesis on a rate table indicate that the device's output matches the average firing rate of vestibular neurons to those in animal models reported in the literature. The proposed design is scalable; the sensing unit, pulse generator, and the current source can be potentially implemented on a single chip using integrated MEMS technology.

Keywords: MEMS, Vestibular Prosthesis, Gyroscopes

1. INTRODUCTION

Sensory prostheses to artificially replace lost sensory function for a number of sensory systems are currently under investigation. For example, cochlear implants use electrical stimulation to restore hearing and provide some relief for patients suffering profound sensorineural hearing loss.[1] Using similar principles, a vestibular prosthesis could provide head orientation information to the nervous system for patients suffering from peripheral vestibular disorders.

The vestibular organ of the inner ear is the major anatomical system to sense motion. The primary function of the vestibular system is to provide information to the brain about the body's motion and orientation. It measures six quantities concerning the spatial orientation including 3-axes angular acceleration and 3-axes linear acceleration. Diminished balance ability, often seen in older adults, poses a serious health risk due to the increased likelihood of the falling.

Several approaches can be considered for improvement of balance sensation and postural control. Appropriate drugs could relief some of the symptoms. Non-invasive exercise has relatively low risk and may also lead to improvement of the vestibular function. If the natural tactile sensitivity and balance control cannot be improved using non-invasive methods, prosthesis might be an alternative way to restore balance function. In balance related prosthetics, sensors such as gyroscopes and accelerometers can sense the motion and provide patients with information about body's orientation. Such a device could be used as a temporary aid during recovery from ablative inner-ear surgery and as a permanent prosthesis for those elderly prone to falls.[2]

At least two categories of vestibular prosthesis might be considered. One approach is to provide the head movement information to the nervous system directly by electrically stimulating the vestibular neural pathways related to spatial orientation. Another approach is to provide the information via sensory substitution through other sensory systems (e.g., tactile, visual, auditory, etc.).[3]

This work falls in the first category. Our goal is to develop an implantable, vestibular neural prosthesis using electrical stimulation. It offers potential opportunity to restore seriously diminished vestibular systems. The

Further author information: (Send correspondence to Prof. Andrei Shkel)
Andrei Shkel: E-mail: ashkel@uci.edu, Telephone: 1 949 824 3843

Smart Structures and Materials 2006: Sensors and Smart Structures Technologies for Civil, Mechanical, and Aerospace Systems, edited by Masayoshi Tomizuka, et al., Proc. of SPIE Vol. 6174, 617414, (2006) · 0277-786X/06/$15 · doi: 10.1117/12.659293

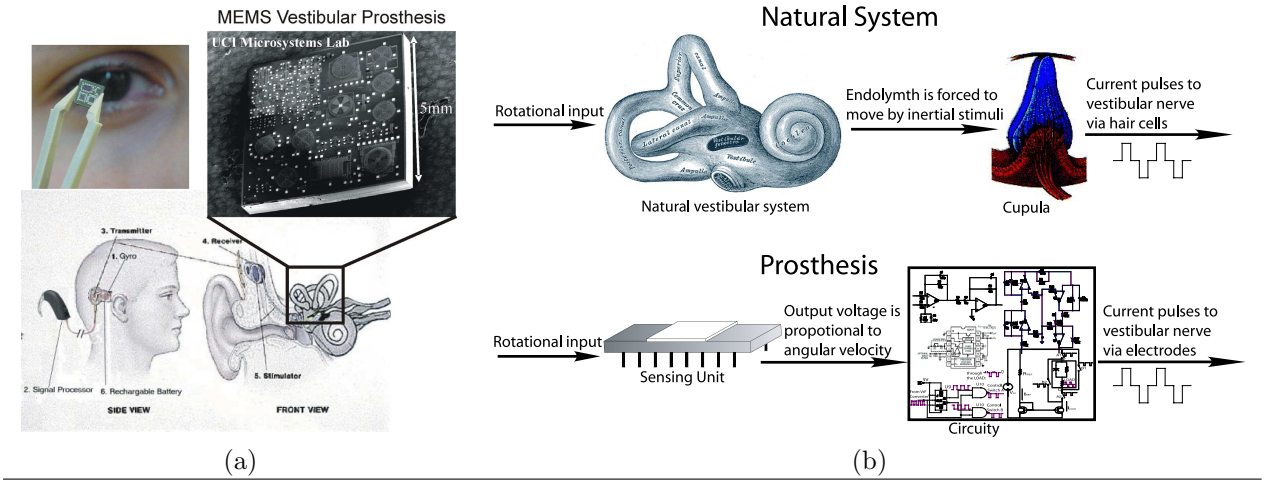

Figure 1. (a) A conceptual model of a totally implantable vestibular prosthesis. The implant is based on 3-axes micro-size gyroscopes integrated alongside with signal conditioning electronics on the same silicon chip; (b) MEMS-based neural vestibular prosthesis is mimicking functionality of the natural vestibular end-organ

long term goal of this research is to explore opportunities for development of a totally implantable MEMS-based electronic device which functions identically to the vestibular system, Figure 1. Using unique feature of the MEMS technology and Integrated Circuit (IC) technology, micromachining can shrink the sensors size by orders of magnitude, reduce the fabrication cost significantly, and allow the electronics to be integrated on the same silicon chip. Figure 1 shows a 5 by 5 millimeter silicon chip developed by UCI's Micro-system lab. The chip includes prototypes of 6 gyroscopes and several linear and angular accelerometers. By merging two advanced technologies of micro-machined gyroscope[4] and cochlear implants,[1] it is possible to build a micro-vestibular neural prosthetics which restores balance function, consumes little power, and can be made in batches.

To the best of our knowledge, there is only one group working on neural semicircular canal prosthesis that has already reported successful interface of the device with vestibular neurons.[5,6] In the reported implementation, an off-the-shelf single axis piezoelectric vibrating gyroscope was used to measure the head rotation and a micro-controller was used to convert rotational information into electrical pulsatile stimulus to provide corresponding stimulus to the nervous system.

The approach reported in this paper is based on a custom design of sensors using the MEMS technology and a custom analog-digital design of the pulse generating unit converting rotational information into electrical stimulus, Figure 1(b). The proposed design can potentially integrate sensors alongside with control electronics on the same silicon chip in a volume smaller than 1 cubic centimeter. Such "balance on-a-chip" system might potentially replace the function of the damaged vestibular end-organ by providing 3-dimensional motion information for people who have permanently lost peripheral vestibular function.

This paper is organized as follows. Section 2 introduces physiology and function of the vestibular system. Section 3 discusses main functional blocks of the proposed vestibular prosthesis. Section 4 presents an engineered prototype of the unilateral vestibular prosthesis and comparing performance of the prototype to the experimentally obtained results on a squirrel monkey model. The paper concludes with discussion about opportunities and challenges which will need to be overcome to realize a totally implantable vestibular prosthesis.

2. VESTIBULAR SYSTEM AND FUNCTION

The properly functioning vestibular system is responsible for a number of reflexes and reactions critical for achieving and maintaining equilibrium of the body and stabilization of images on the retina as the head and body are moved. The vestibular system comprises the non-acoustic portion of the inner ear and consists of three semicircular canals and two otolith structures called the utricle and the saccule. The sense organs of the semicircular canals detect rotational head movements, while the sense organs of the saccule and utricle detect

linear movements of the head. All of these organs have small sensory hair cells that send pulses through the nerves to the brain, where information about head movement is combined with information from the eyes, muscles, and joints, which are then interpreted.

Angular accelerations stimulate the semicircular canals. The semicircular canals are three approximately circular canals whose planes are mutually orthogonal. Each canal is filled with fluid, endolymph, which, by virtue of its inertia, flows through the canal whenever an angular acceleration in the plane of the canal is experienced by the head. Flow of the endolymph deflects the cupula, a flapper-like valve which seals an expanded portion of each duct called the ampulla. Displaced endolymph Bends the tiny hairs of sensory cells (stereocilia) inside the canals and chambers, initiating nerve impulses that pass along the vestibular nerve to the brain. The impulses provide information to the brain about changes in head position.

The rotational perceptual threshold in humans was determined to be between $0.1^0/sec$ and $2^0/sec$.[7] Strictly speaking, the endolymph responds to the inertial forces induced by angular acceleration, however due to over-damped mechanical structure of the endolymph-cupula biomechanical system, angular velocity is often used for defining the perceptual threshold. Montandon[8] determined that the acceleration threshold is $1^0/sec^2$ in healthy individuals, but greater than $6-7^0/sec^2$ in patients with vestibular dysfunction. It should be noticed, however, that perceptual thresholds are different for different rates of acceleration and vary from person to person. The reported sensation limits set the sensitivity requirements for the vestibular prosthesis.

Another critical physiological parameter is the firing rate of neurons and relation of the firing rate to the head rotation/translation. The average firing rate of regular vestibular units has been reported as 60 spikes/s in the guinea pig[9] and 90 spikes/s in the squirrel monkey.[10] The firing frequency increases when a semicircular canal responds to rotation in one direction, and decreases in the other direction. In the guinea pig, the average sensitivity is roughly 0.3 spike/s per $1^0/sec$ for regular afferents and 0.7 spike/s per $1^0/sec$ for irregular afferents.[9] The results in relation of the firing rate to the head rotation/translation set the requirement for the pulse generating unit determining the rate of electrical stimulation in the vestibular nerve.

3. SYSTEM DESIGN

The purpose of the semicircular canal prosthesis is to restore balance function. Ideally, the prosthesis will be able to sense motion with sufficient precision and to deliver signal to the central neural system matching signal that the natural organ would generate, thus mimicking the dynamic vestibular function, Figure 1(b). The device includes three main functional units - a sensing unit, a pulse generator, and a stimulator, Figure 1(b).

The sensing unit includes a gyroscope, a low-pass filter and a differentiator; it detects the motion of the head and sends out the analog voltage signal proportional to angular acceleration about the sensing axis. The pulse generator consists of a transfer function unit and a voltage-to-frequency converter; it generates monophasic voltage pulses based on a selected mathematical model describing biomechanics of the vestibular organ. The current source includes monophasic-to-biphasic converter (Smith triggers and analog switches) and a current mirror; they convert the monophasic voltage pulses to biphasic, charge-balanced, cathodic-first current pulses which can be used to stimulate vestibular neurons.

3.1. Sensing Unit

The discussed unilateral prosthesis is utilizing a custom made single-axis Micro-Electro-Mechanical System (MEMS) gyroscope, developed by UCI Microsystems Laboratory,[12] Figure 2(a). Using MEMS technology, big and expensive mechanical devices can now be realized as micron-size structures integrated on one chip, together with electronics,.[13] The gyroscope prototypes used in these experiments were packaged together with preamplifiers in the same package by direct wire bonding Figure 2(b). The gyroscope is approximately $2\times 2mm^2$ in size with a minimum features $5\mu m$.

Our micromachined gyroscopes use vibrating element to measure rotational velocity based on the Coriolis principle.[15]

In the basis of operation, the proof-mass, which constitute the active portion of the sensor, is driven by an oscillator circuit at a precise amplitude X_D and high frequency ω_n, $x(t) = X_D sin(\omega_n t)$. When subjected to a

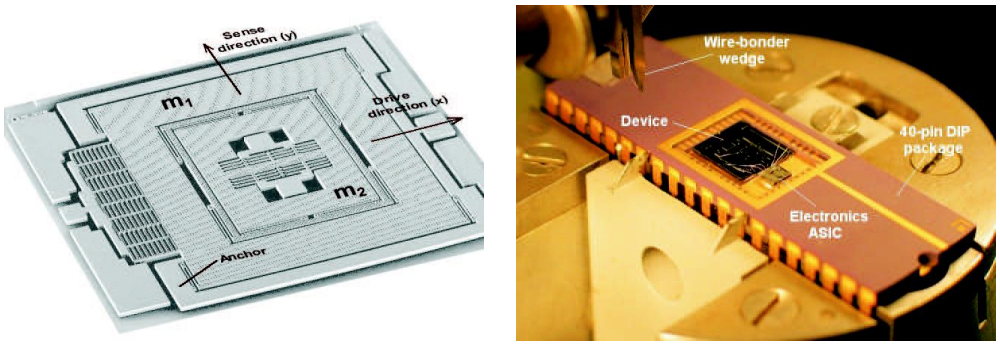

(a) (b)

Figure 2. (a) Scanning Electron Micrograph (SEM) of a prototype bulk-micromachined gyroscope[14]; (b) A prototype gyroscope packaged together with preamplifiers in the same package by direct wire bonding

rotation with angular velocity Ω, the proof-mass will be subjected to the Coriolis force. The resultant Coriolis force is perpendicular to both the input rate and the instantaneous radial velocity in the drive direction. This produces a motion of the proof-mass, $y(t)$ in direction perpendicular to its initial oscillation:

$$\|y(t)\| = \frac{2X_D \Omega Q}{\omega_n} \tag{1}$$

This expression shows that the output sense deflection is proportional to the input angular velocity. The gyroscope response is also directly proportional to quality factor Q of the device. To improve performance of micromachined gyroscopes, the devices have to be vacuum packaged to achieve high amplitude of response in the sense direction. Detection of the Coriolis response is extremely challenging, since it requires measurement of picometer-scale oscillations in the sense mode, while the proof-mass oscillates with tens of microns amplitude in the drive mode. Synchronous demodulation technique is commonly used to tackle this problem. A high-frequency carrier signal is imposed on the structure. An array of differential capacitors is used to detect pico-meter scale deflections due to the Coriolis induced motion. The difference of the outputs of the differential amplifiers is amplitude demodulated at the carrier signal frequency, yielding the Coriolis response signal at the driving frequency.

The described principle of operation is not the only option for implementation of MEMS gyroscopes. Multi-degree of freedom gyroscopes and vibratory gyroscopes with rate integrating capabilities have been also developed.[15]

For the demonstration purposes we considered a MEMS gyroscope utilizing a novel 3-DOF structure, designed and implemented by the UCI Micro-systems laboratory Figure 2,.[14] The overall 3-DOF micromachined gyroscope is formed by a 2 DOF drive mode oscillator and a 1 DOF sense mode oscillator. This architecture allows to improve sensitivity while maintaining the robust operation characteristics. The device was operated in air (not vacuum packaged). The drive signal of 10 V DC bias and 2 V AC was applied on the drive mode parallel plate actuators. The device was operated on the lower drive-mode resonance pick, at approximately 1 kHz. A 20 kHz carrier signal was imposed on the gyroscope structure, which is the common-mode of the differential capacitive bridge in the sense mode. The current output from each sensing capacitor due to the carrier signal is converted into a voltage signal and amplified using two transimpedance amplifiers with $1M\Omega$ feedback resistors. The difference of the outputs is amplitude demodulated at the carrier signal frequency using a lock-in amplifier, yielding the Coriolis response signal at the driving frequency. The Coriolis signal was demodulated at the driving frequency, yielding the DC voltage output proportional to the angular rate input, Figure 3.

Using the synchronous demodulation technique, a sensitivity of $0.0694 mV/^0/sec$ and a noise floor of $0.211 mV/\sqrt{Hz}$ at 50 Hz bandwidth was measured. This yields a measured resolution of $3.05^0/sec/\sqrt{Hz}$ at 50 Hz bandwidth.

The gyroscope is sensing any type of angular rotation (constant or non-constant rotational rate), while the natural vestibular organ is only responding to the angular acceleration. Thus, in order to mimic the natural organ,

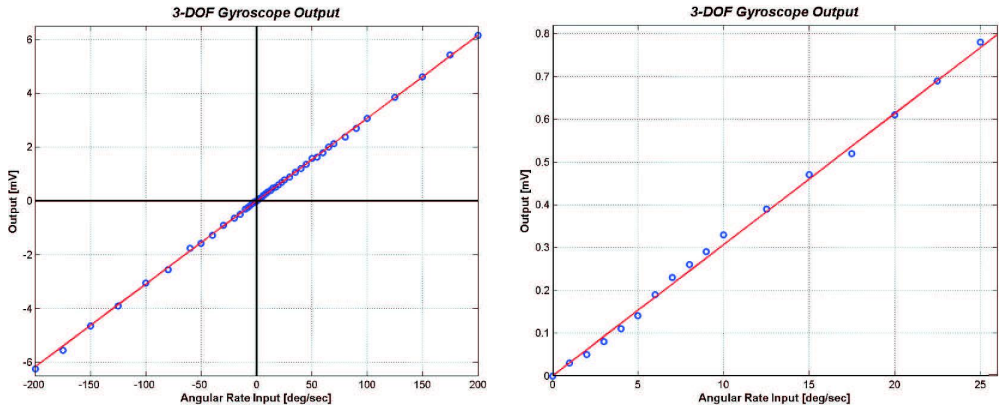

(a) (b)

Figure 3. The angular rate input vs. voltage output plot obtained from the 3-DOF gyroscope with 2-DOF sense mode (a) in the range -200^0/sec to -200^0/sec; (b) in the range 0^0/sec to 25^0/sec

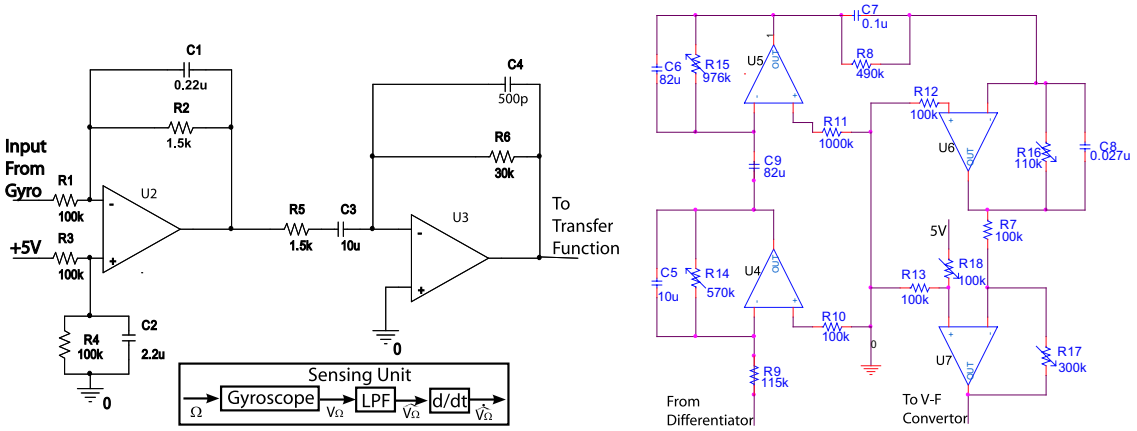

(a) (b)

Figure 4. (a) Sensing Unit includes a gyroscope and low-pass filter and differentiator; (b) Transfer function mimicing dynamics of the semicircular canals of the squirrel monkey model(reported in[10])

the supporting circuit differentiates the output voltage of the gyroscopes to produce the signal proportional to the angular acceleration. In our implementation, the circuit is utilizing a low-pass filter before the differentiator for minimizing the effect of high-frequency noise, Figure 4(a).

3.2. Pulse Generator

The gyroscope detects the motion of the head and sends the analog voltage signal to a pulse generator. The pulse generator consists of a transfer function unit emulating dynamics of the natural vestibular organ, Figure 4(a). It uses a fifth order transfer function to convert input angular acceleration to the frequency shift from the rest firing rate of the vestibular neurons. The unit than uses a Voltage-to-Frequency converter to provide a more physically relevant output.

The transfer function emulating dynamics of the natural vestibular organ is modeled as a linear torsion-pendulum system.[16,17] In this model, the cupula and endolymph are treated as a heavily damped, second-order linear system, where the cupula angular deflection $\varepsilon(t)$ is related to angular acceleration $\alpha(t)$ by differential equation[16,17]

$$\Theta \frac{d^2\varepsilon(t)}{dt^2} + \Pi \frac{d\varepsilon(t)}{dt} + \Delta\varepsilon(t) = \Theta\alpha(t) \tag{2}$$

with $\tau_1 = \Pi/\Delta$ and $\tau_2 = \Theta/\Pi$ are two time constants defined by morphology and material properties of the end-organ. A more complex linear model defining the relationship between the input angular acceleration and overall change in firing rate of neurons is described by

$$H(s) = \frac{\tau_A s}{1+\tau_A s} \cdot \frac{1+\tau_L s}{(1+\tau_1 s)(1+\tau_2 s)}, \tag{3}$$

where τ_1 and τ_2 and two time constant of the pendulum model described above, τ_A is related to the level of neuron adaptability, and τ_L is the dynamical-electrical time constants.[10]

Experimentally obtained results in[10] for the squirrel monkey model estimate $\tau_1 = 5.7sec$, $\tau_2 = 0.003sec$, $\tau_A = 80sec$, and $\tau_L = 0.049sec$. We use these experimentally defined time-constants for the design of equivalent circuit, Figure 4(b).

Four operational amplifiers are used to implement the transfer function relating the input angular acceleration and the frequency shift form the rest firing rate of the vestibular neurons (the firing rate when there is no rotational stimulus). The transfer function is separated in three parts: $H(s) = H_1(s) \cdot H_2(s) \cdot H_3(s)$, where

$$\begin{aligned} H_1(s) &= K_1 \frac{1}{1+\tau_1 s} = -\frac{R_{14}}{R_9 \cdot (1 + R_{14} \cdot C_5 \cdot s)} \\ H_2(s) &= K_2 \frac{\tau_A s}{1+\tau_A s} = -\frac{R_{15} \cdot C_9 \cdot s}{1 + R_{15} \cdot C_6 \cdot s} \\ H_3(s) &= K_3 \frac{1+\tau_L s}{1+\tau_2 s} = -\frac{R_{16} \cdot (1 + R_8 \cdot C_7 \cdot s)}{R_8 \cdot (1 + R_{16} \cdot C_8 \cdot s)} \end{aligned}$$

K_1, K_2, K_3 are adjustable gain constants. The components of the transfer function H_1, H_2, and H_3 are defined by the operational amplifiers, U_4, U_5, and U_6 in Figure 4(b), respectively. The transfer function produces voltages proportional to the shift from the rest firing rate of vestibular neurons.[10] An additional operational amplifier U_7 is used after the transfer function $H(s)$ to adjust the voltage corresponding to the rest firing rate. For our particular implementation, we used

$$U_{7out} = -\frac{R_{17}}{R_7} \cdot U_{7in} + \frac{R_{13} \cdot (R_7 + R_{17})}{R_7 \cdot (R_{13} + R_{18})} \cdot 5(Volt)$$

with the values of the active components defined in Figure 4(b). In this implementation, U_{7in} is proportional to displacement from rest firing rate and U_{7out} is proportional to firing rate. If there is no rotational stimulus, U_{7in} is equal to zero, then the scaled zero shift voltage U_{7out} becomes 2 Volt.

A Voltage-to-Frequency (V-F) converter (AD537) is used to convert the voltage signals corresponding to the shift from the rest firing rate to the equivalent frequency pulses. The corresponding input/output relationship is[18]

$$F_0 = \frac{V_{IN}}{10 R_{19} C_{10}} \tag{4}$$

In our implementation we choose $R_{19} = 10k\Omega$ and $C_{10} = 0.1\mu F$ resulting in $F_0 = 100 \cdot V_{IN}(Hz)$. The output is binary - 0 Volt (OFF) and 5 Volt (ON), and the duty time is 50%. For the selected parameters, the static F_0 is $100(Hz/Volt) \times 2(Volt) = 200Hz$.

3.3. Current Source

The current pulses sent via neurons to brain are delivered by ion flow, so that the total charge sent to the nerve should be zero. Since tissue impedance is changing over time, a voltage source may not maintain constant current for charge delivery. Thus, a stimulation with current source, instead of a voltage source, is required to transmit signals via neurons. The overall charge sent via neural fibers should be zero (e.g.,[1]), so that the integration of the current over time is zero. If this condition is not satisfied, the neuron could be destroyed. In order to satisfy these constrains, monophasic voltage signal has to be changed to biphasic current signal.

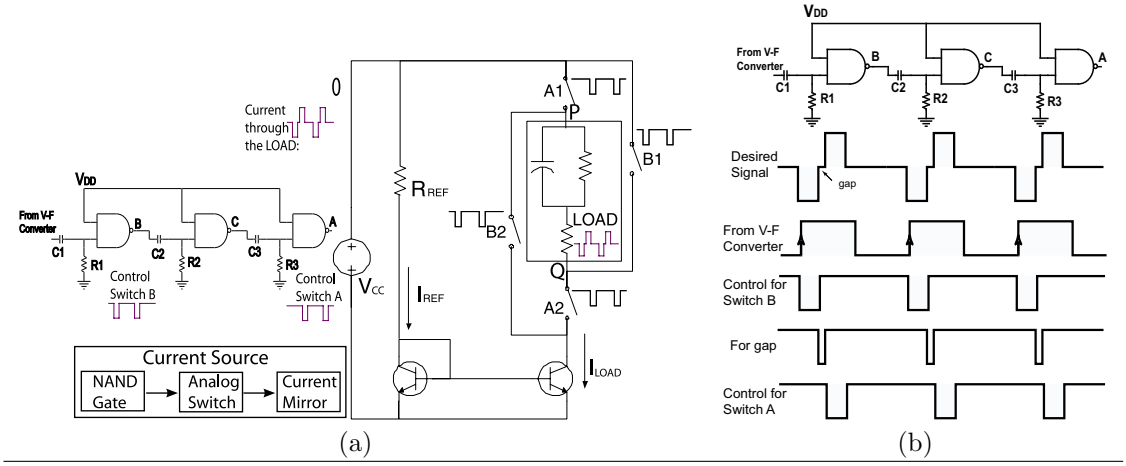

Figure 5. (a) Current source converting monophasic voltage pulses to biphasic current pulses; (b) Control signal of the switches using Smith triggers

Figure 5(a) shows our conceptual implementation of the current source, which includes a current mirror, analog switches and Smith triggers. The analog switches and Smith triggers convert monophasic signal to biphasic signal, and the current mirror provides current output that is not affected by the load impedance.

The biphasic current stimulus is produced from the monophasic voltage signal utilizing V-F converter by "mirroring" the input signal using four components: J/K converter, NAND logical gate, analog switches, and current mirror, Figure 5(a). The left side of Figure 5(a) shows an J/K Flip-Flop (U_9, 74LS73) followed by two NAND Gates (U_{10}, CD4093BE). The clock(CLK) for the J/K converter comes from Voltage-to-Frequency converter, so that the clock frequency is proportional to firing rate and corresponds to the rotations sensed by the gyroscope. The J and K input are all high voltages (5V), so that the output Q toggles when there is a "Rising Edge" trigger in the clock. It means that the frequency of the output Q, $\overline{Q}$, is half of the input clock (CLK). The logic for the control signal of analog switches are switch $A = \overline{CLK \cap Q}$ and switch $B = \overline{CLK \cap \overline{Q}}$. An analog switch ($U_{11}$, CD4053) uses these two control signals to control the connectivity of switches A_1, A_2, B_1, and B_2.

The right side of Figure 5(a) shows the current source configuration such as A_1 and A_2 are connected, while B_1 and B_2 are disconnect, forming a typical current mirror with $I_{LOAD} \approx I_{REF}$ (holding when the condition $R_{LOAD} < R_{REF}$ is satisfied). Since V_{CC} and R_{REF} are fixed in the design, the corresponding I_{REF} is guaranteed to be fixed. When A_1 and A_2 are connected, and B_1 and B_2 are disconnected (low control voltage makes the switch connected and high control voltage makes the switch disconnected), the current flows from P to Q, Figure 5(a). In contrast, when A_1 and A_2 are disconnected, and B_1 and B_2 are connected, the current flows from Q to P. When all the four switches are disconnected, there will be no current flow through the load. Such scheme of analog logical switches allows to convert monophasic voltage signal to biphasic current signal. In the proposed design, the amplitude of I_{LOAD} may be changed by adjusting R_{REF}.

The Pulse Duration (PD) is defined by the time constant of each smith trigger, as long as the output voltage increases before the input voltage drops, i.e., the pulse duration is not influenced by the input frequency.

For each NAND Gates, Figure 5(b), when one of the input is kept high, another input (V_1) governs the output. As soon as the voltage at V_1 falls below V_{T-} (1.8Volt), V_{OUT} changes from low to high. So the pulse duration (PD) in V_{OUT} can be calculated by

$$e^{\frac{PD}{\tau}} = \frac{V_{DD}}{V_1} \tag{5}$$

The maximum neuron firing rate is around 250Hz,[6] so the minimum duration for each firing cycle is around 4ms. Since the pulse duration in V_{OUT} should be less than half of the firing cycle, the PD+ and PD- are designed

to be 1ms. Substituting 5 Volt in V_{DD} and 1.8 Volt in V_{T-}, time constant τ can be calculated from Equation (5)

$$\tau = \frac{PD}{ln(\frac{V_{DD}}{V_1})} = \frac{PD}{ln(\frac{5}{1.8})} = 1.0217$$

Three Smith triggers are used in our implementation to achieve control signal for the switches. In Figure 5(b), the rising edge from the output of the voltage-to-frequency converter triggers a negative pulse at point A, the rising edge from the voltage at point A triggers a negative pulse at point B, and the rising edge from point B triggers a negative pulse at point C. The pulse duration is defined by the time constant of each Smith trigger, as long as the output voltage increases before the input voltage drops. Control signals at point A and point B determine the state of analog switches, A and B, respectively. Using the scheme, the biphasic current pulses are generated and are kept constant during the stimulation. The proposed scheme allows to adjust pulse durations (e.g., if desired by an experiment on different subjects). The pulse frequency can be adjusted by changing resistances R_1 or R_3, Figure 5(b). The pulse magnitude can be adjusted by modifying R_{REF}, Figure 5(a).

The electrical properties of a biological tissue can be modeled by an equivalent circuit as a resistor and a capacitor in parallel, plus a resistor in series. The values of the resistors and capacitor in this model are fluctuating. By using the current mirror illustrated in Figure 5(a), the voltage across the LOAD may change due to changes in impedance of the tissue, however the current through the LOAD will not be affected.

4. EXPERIMENTAL RESULTS

Based on the discussed design, a circuitry prototype is implemented on a Printed Circuit Board (PCB), Figure 6. It consists of a sensing unit which includes a z-axis gyroscope, a low-pass filter and a differentiator; a pulse generating unit which includes a transfer function unit and a voltage-to-frequency converter, and a current source which includes Smith triggers, analog switches and a current mirror. Two nine volt batteries are used as a power supply for the prototype circuitry and the sensor. Nine potentiometers are utilized to adjust for the resistance parameters, including four time constants in the transfer function (τ_A, τ_1, τ_2, and τ_L), rest firing rate, gain of the transfer function, positive and negative pulse duration, and magnitude of the current pulse.

4.1. Time Domain Response

A fragment of the circuit response to sinusoidal voltage input is illustrated in Figure 7(b) at three different time scales (500ms, 50ms, 2ms in (a), (b), (c), correspondingly). The voltage response is recorded using Virtual Bench 2.1.1 (a Labview program by National Instruments) through a data acquisition board (National Instruments BNC-2110). Then the data was saved as the text file, which was subsequently imported and analyzed in Matlab.

Legend (1) in Figure 7(b) is generated from a signal generator at 2Hz frequency, 0.5V peak amplitude, and 2.43Volt offset, and it acts as the output from the gyroscope. The gyro calibration shows that the corresponding motion is harmonic rotation with zero offset, 2Hz frequency and 40degree/second peak amplitude. Legend (2) shows the voltage signal after the transfer function unit, and it is proportional to the pulse rate of legend (3), Figure 7(b), and (a). For the convenience of recording, voltage across the load (Legend 3) is measured. The current through the load is obtained by dividing the voltage by the load impedance, which in turns consists of biphasic, charge-balanced, and cathode-first pulses. Changing the load impedance, the amplitude of voltage pulses changes, and the amplitude of the current pulses is kept constant. Figure 7(b), (b) and (c) scale the time duration down to 50ms and 2ms, correspondingly. In Figure 7(b), chart (c) illustrates the voltage pulses across the load. Three parameters of the pulse shape can be adjusted for the best performance of the stimulator, i.e., positive and negative pulse duration (PD+, PD-) and pulse magnitude (Mag).

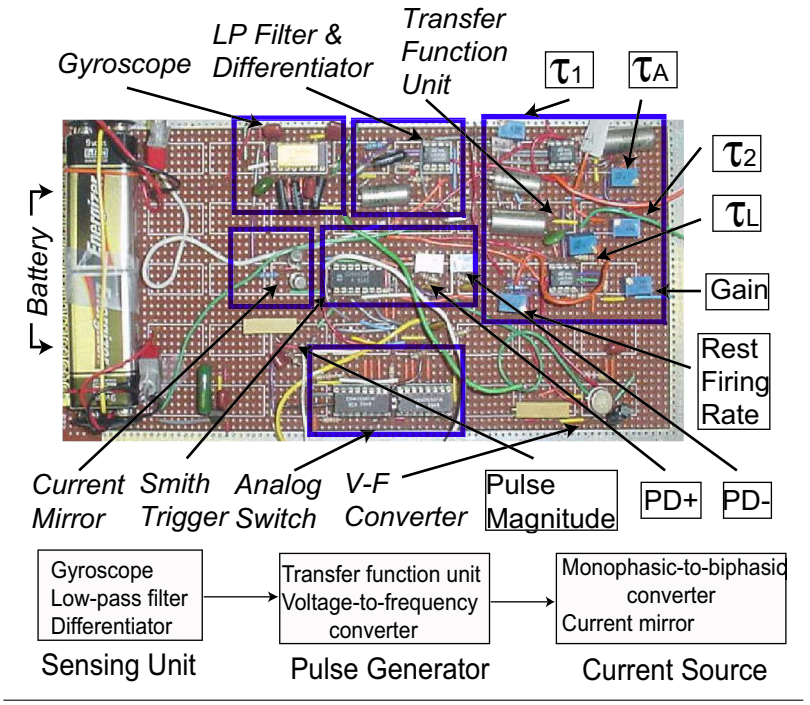

Figure 6. Printed Circuit Board (PCB) prototype of the electrostimulatory unilateral prosthesis

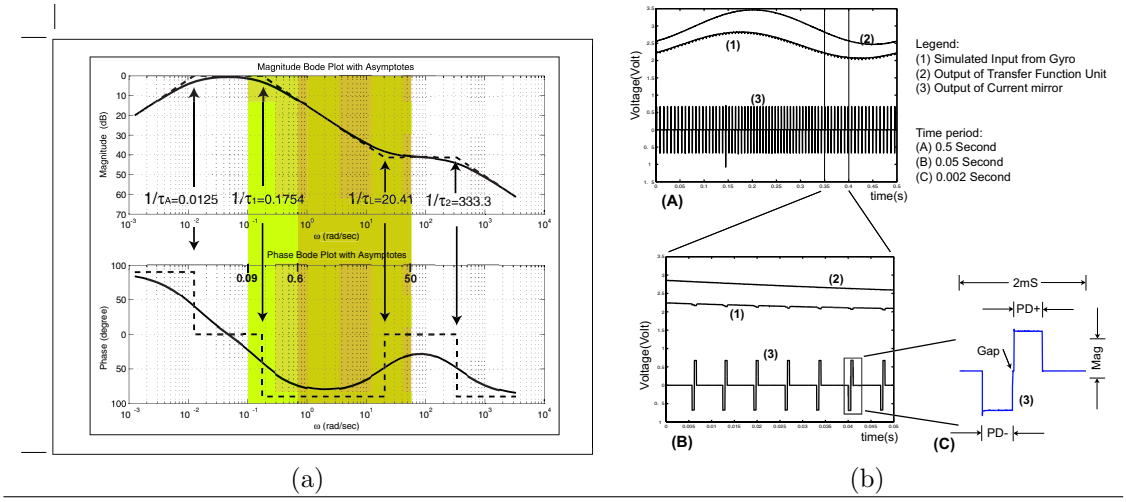

(a) (b)

Figure 7. (a) Bode plot with asymptotes of the mathematical model; (b)Circuitry response to harmonic inertial stimuli

4.2. Parameter Sensitivity

Figure 7(a) illustrates a bode plot with asymptotes of the mathematical model H(s), Equation 3. The continuous line is the actual response of the mathematical model in the frequency domain. The four time constants characterize the break points of the gain and the phase, defined by dashed asymptotes, Figure 7(a). The value of the four time constants are shown in the transfer function H(s)

$$H(s) = \frac{\tau_A s}{1+\tau_A s}\frac{1+\tau_L s}{(1+\tau_1 s)(1+\tau_2 s)} = \frac{80s}{1+80s}\frac{1+0.049s}{(1+5.7s)(1+0.003s)}$$

In our implementation, $1/\tau_A, 1/\tau_1, 1/\tau_2$, and $1/\tau_L$ are equal to 0.0125 rad/s, 0.1754 rad/s, 333.3 rad/s, and 20.42 rad/s, correspondingly.

In different subjects, the response of the natural vestibular system under the same inertial condition may be different. The proposed architecture of the prosthesis allows to adjust parameters, making the response of the circuit to fit the response of the natural vestibular system.

4.3. Response of the Prosthesis

Performance of the unilateral vestibular prosthesis was compared to the experimentally obtained results in[10] on a squirrel monkey animal model. In the experiment the animal was mounted in a structure, so that the center of the head was coincident with the axis of rotation and the horizontal canal is in horizontal plane. Sinusoidal rotations with frequency $0.1 - 8Hz$ were sequentially applied and response of neurons firing in the vestibular nerve were monitored and recorded. In our experiment, we initially placed our prototype on a rate table and applied a constant rotational input. This allowed us to build the input/output relations for the gyroscope. After that we modeled the response of the gyroscope under the same rotational conditions as those reported in.[10] A fragment of the prosthesis response to inertial stimulus is illustrated in Figure 8(a)

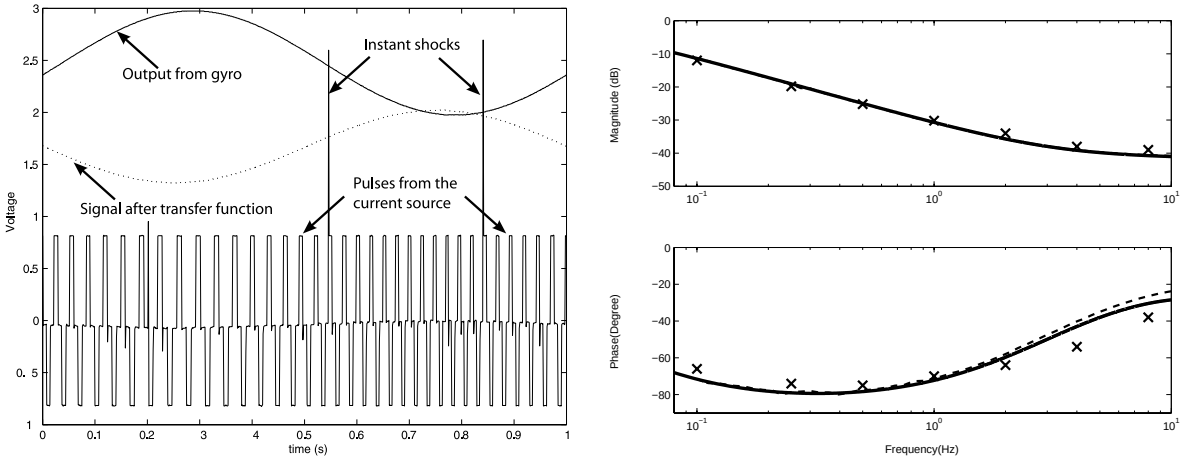

Figure 8. (a) Response of the prosthesis to the harmonic inertial excitation; Comparison of response of the circuitry and of the natural vestibular system in the squirrel monkey experiments reported in the literature[10]

The continuous line in Figure 8 (a) is a sinusoidal input rotation of the rate table as it were measured by the sensing unit (gyroscope) of the prosthesis. The dashed line is the analog signal after the input from the gyroscope was fed through the transfer function of the pulse generating unit. The fixed amplitude pulses are supperimposed in the same figure to illustrate dependence and similarity of the signal provided to the vestibular nerve by the natural vestibular system and the developed vestibular prosthesis. For the illustration purposes the input rotation was harmonic with the frequency $1Hz$ and with the acceleration amplitude $250^0/sec^2$. The output biphasic current pulses generated by the prosthesis are $40spikes/sec$ for the resting firing rate and with maximum at $50spikes/sec$ and minimum at $30spikes/sec$. Note that the resting firing rate and sensitivity can be easily scaled using the amplifier U_7. Instant shocks in Figure 8 (a) can be attributed to conversion of the digital signal to analog signal. Such short-term shocks are unavoidable and can be minimized by adding a small capacitor parallel to the load.

In Figure 8 (b) we provide a side-by-side comparison between the experimental results on squirrel monkey[10] and the design vestibular prosthesis. Data points marked with(X) represent experimentally measured responses in firing of nerves in semicircular canals of the squirrel monkey animal model.[10] The comparison is performed for the harmonic angular acceleration with frequencies between 0.1 Hz and 8 Hz. The gain results demonstrate a very close match between two experiments, however there is a slight phase shift between the data obtained

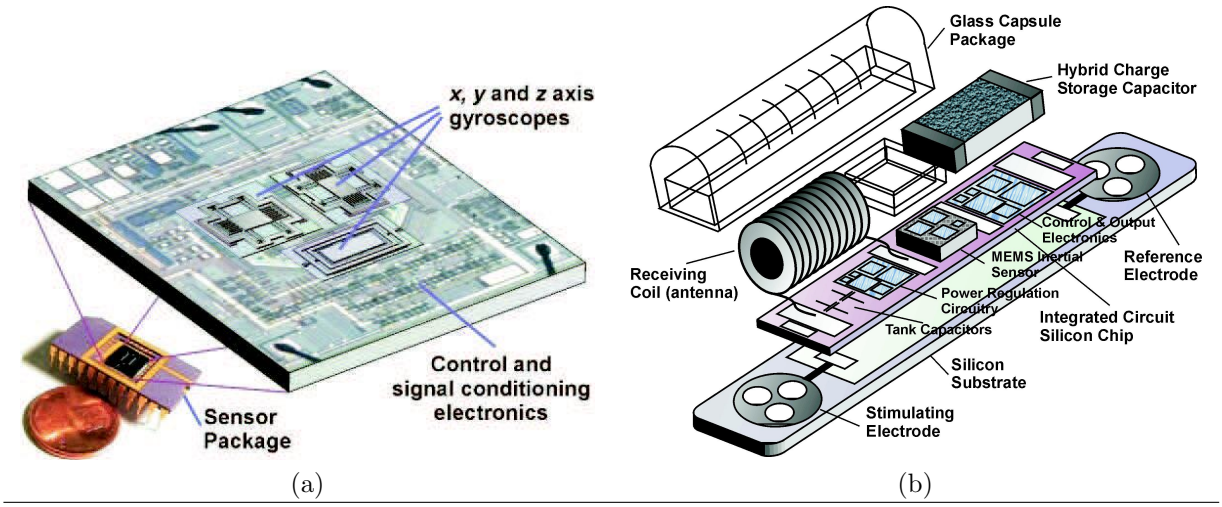

Figure 9. (a) Conceptual illustration of the final inertial measurement unit with integrated electronics (b) Structure of the totally implantable vestibular prosthesis showing the silicon substrate, receiver circuitry, 6-DOF inertial sensors, vacuum packaging cup, and glass capsule.

from the prosthesis and the animal experiment. This miss-matching is negligible at low frequencies and it gradually increasing at higher frequencies. We believe higher order mathematical models of the biomechanics of the vestibular organ are required to capture this phenomena.

5. REMAINING ISSUES AND FUTURE DIRECTIONS

This paper discusses initial implementation and experimental verification of the prototype of the electronic prosthesis mimicking the function of a unilateral semicircular canal. Our preliminary results demonstrated a possibility of designing a MEMS electronic system which can closely match the response of the natural vestibular organ in the presence of unilateral rotation.

Our next step is to demonstrate on live animal models a possibility for sensory substitution. We believe, damaged, or temporarily disabled, vestibular organ can be effectively replaced by the electrostimulatory prosthesis with the proposed architecture. The surface mount hybrid techniques will be initially used to reduce the size of the overall system, followed by implementation of the system on a single chip, Figure 9(a). Low power consumption electronics designs will be also explored for the next generation of the vestibular prosthesis. A totally implantable version of the prototype is currently explored by this group. A new system components are planned to be added to the next generation prototype, including wireless communication capabilities, wireless gain adjustment capabilities, and wireless power supply. The package structure will consist of (1) a silicon substrate supporting a stimulating electrode at each end and providing multiple feedthroughs; (2) Receiver circuitry along with its hybrid chip capacitor and receiver coil; (3) a sensing unit encapsulated in a vacuum environment; and (4) a glass capsule that is electrostatically bonded to the substrate to protect the receiver circuitry, sensors, and hybrid elements from body fluids, Figure 9(b).

It is realized however, that successful implementation of the vestibular prosthesis will require not only innovative engineering solution but also novel surgical approaches. The procedures of implantation and interface with vestibular nerves should be relatively easy and reproducible. The bundle of the vestibular nerve is very close to the facial and hearing nerves, thus the procedures of implantation should minimize, or better eliminate, the risk of adjacent nerve injuries, should ensure residual hearing preservation, and minimize morbidity. There are a lot of questions still open.

Even though some preliminary results already available in the literature, we will expect a lot of future activities in trying to understand the issues of the most effective stimulation of the vestibular nerve and achieving vestibular selectivity of the stimulation.

6. ACKNOWLEDGMENT

Author would like to acknowledge Dr. Acar for contribution in development of MEMS gyroscope, J. Liu for work on implementation of Pulse Generator and Current Source, and Fan-Gang Zeng for useful discussions on electrical stimulation.

This project was partially supported by NSF CAREER award CMS-0449442.

REFERENCES

1. S.U. Ay, F.-G. Zeng, and B. Shen, "Hearing with Bionic Ears," *IEEE Circuits and devices*, vol. 5, pp. 18–23, 1997.
2. C. Wall and M. Weinberg, "Balance prostheses for postural control," *Journal of Neurophysiology*, vol. 22(2), pp. 84–90, 2003.
3. M. Weinberg, J. Borenstein, J. Connelly, A. Kourepenis, P. Ward, and J. Heiertz, "Application of Draper/Boeing micromechanical inertial instruments," *Sensors Expo'98*, vol. CSDL-P-3673, 1998, oct., Chicago, IL.
4. A. M. Shkel and R. T. Howe, "Micro-machined angle-measuring gyroscope," U.S. Patent 6,481,285, Nov. 19, 2002.
5. W. Gong and D. Merfield, "Prototype neural semicircular canal prosthesis using patterned electrical stimulation," *Ann. of Biomed. Eng.*, vol. 28, pp. 572–581, 2000.
6. ——, "System design and performance of a unilateral horizontal semicircular canal prosthesis," vol. 49, pp. 175–181, Feb. 2002.
7. A. Benson, "Thresholds for the perception of whole body angular movement about a vertical axis," *Aviat., Space Envi-ron.Med.*, vol. 60, pp. 205–213, 1989.
8. A. Montandon, "A new technique for vestibular investigation," *ACTA Otolaryngology*, vol. 39, p. 594, 1954.
9. I. Curthoys, "The response of primary horizontal semicir-cular canal neurons in the rat and guinea pig to angular acceleration," *Exp. Brain Res.*, vol. 47, p. 286294, 1982.
10. J. M. Goldberg and C. Fernandez, "Physilology of peripheral neurons innervating semicircular canals of the squirrel monkey. II. Response to sinusoidal stimulation and dynamics of peripheral vestibular system," *J. Neurophysiol.*, vol. 34, pp. 661–675, 1971.
11. J. Liu, A. M. Shkel, K. Nie, and F. Zeng, "Circuit with adjustable parameters mimicking function of the national vestibular end-organ," in *Proc. of the 1st International IEEE EMBS Conference on Neural Engineering*, Capri Island, Italy, Mar. 2003.
12. *http://mems.eng.uci.edu*, uCI Microsystems Laboratory.
13. A. Shkel, "Micromachined gyroscopes: Challenges, design solutions, and opportunities," *2001 SPIE Annual International Symposium on Smart Structures and Materials*, 2001, (Invited Paper) March, 2001, Newport Beach, CA.
14. C. Acar, *"Robust Micromachined Vibratory Gyroscopes"*. Ph.D. thesis, Dept. of MAE, University of California - Irvine, 2004.
15. A. Shkel, C.Acar, and C. Painter, "Two types of micromachined vibratory gyroscopes," *Int. IEEE Sensors Conference*, Oct. 2005, irvine, CA, USA.
16. W. Steinhausen, "ber den nachweis der bewegung der cupula in der intakten bogengangsampulle des labyrinthes bei natrlichen rotatorischen und calorischen reizung," *Arch. Ges. Physiol.*, vol. 228, pp. 322–328, 1931.
17. von A. A. Egmond, J. Groen, and L.B.W.Jongkees, "The mechanics of the semicircular canal," *J. Physiol., London*, vol. 110, pp. 1–17, 1949.
18. I. Analog Devices. (2000) Ad537 reference data sheet. [Online]. Available: http://www.analog.com